International Journal of Remote Sensing

ISSN: 0143-1161 (Print) 1366-5901 (Online) Journal homepage: www.tandfonline.com/journals/tres20

# Water interception by canopies for remote sensing based evapotranspiration models

N. Ghilain, A. Arboleda, J. M. Barrios & F. Gellens-Meulenberghs

**To cite this article:** N. Ghilain, A. Arboleda, J. M. Barrios & F. Gellens-Meulenberghs (2020) Water interception by canopies for remote sensing based evapotranspiration models, International Journal of Remote Sensing, 41:8, 2934-2945, DOI: 10.1080/01431161.2019.1698072

**To link to this article:** https://doi.org/10.1080/01431161.2019.1698072

INTERNATIONAL JOURNAL OF REMOTE SENSING
2020, VOL. 41, NO. 8, 2934–2945
https://doi.org/10.1080/01431161.2019.1698072

Taylor & Francis
Taylor & Francis Group



# Water interception by canopies for remote sensing based evapotranspiration models

N. Ghilain, A. Arboleda, J. M. Barrios and F. Gellens-Meulenberghs

Meteorological and Climatological Research, Royal Meteorological Institute of Belgium, Brussels, Belgium

**ABSTRACT**

Evaporation of intercepted water by canopies accounts for a non-negligible portion of total land surface evapotranspiration. While monitoring evapotranspiration from space technology is increasingly demanded, most evapotranspiration retrieval algorithms face the problem of providing accurate estimation of evaporation from canopy interception. Because of the operations constraints or of the uncertain quality of the near-real-time rainfall estimates from satellites, the implementation of a diagnostic method is preferred to a dynamical model based on a differential equation ruling the evolution of the water storage on the canopy. In this contribution, an empirical model detecting and quantifying intercepted water on canopies, based on one meteorological variable, is optimized with forecasts from a general circulation model. This diagnostic model of interception is implemented in an evapotranspiration retrieval algorithm using mostly space measurements and its impact is commented.

**ARTICLE HISTORY**
Received 7 December 2017
Accepted 25 March 2019

## 1. Introduction

Evapotranspiration is the combination of the plant transpiration, bare soil evaporation, evaporation from water surfaces, including rivers and lakes, and evaporation from water intercepted by the vegetation. Indeed, leaves and needles can store water on their surface. This water can be either intercepted from rainfall, or from dew deposition usually occurring during the night, when plants get cooler than the surrounding atmosphere.

Evaporation of rain interception by the canopy can largely contribute to the total evaporation at seasonal and regional scale over northern Europe and equatorial forest Miralles et al. (2010). Therefore, there is a need to include the modelling of evaporation from rain interception in every model aiming at estimating evapotranspiration.

Most land surface models that predict the evapotranspiration use a 'Gash-type' model (Gash (1979)) to simulate the evolution of the interception reservoir on the canopy. Its input is the rainfall data, evaporation rate and the canopy storage capacity, and it evaluates the quantity of water stored on the canopy and then balances with the loss due to evaporation. It requires solving equations using previous time steps and an estimation of the rainfall rate and duration.

**CONTACT** N. Ghilain nicolas.ghilain@meteo.be Meteorological and Climatological Research, Royal Meteorological Institute of Belgium, 3 Avenue circulaire, Brussels, Belgium

There is an increasing interest in having the evapotranspiration retrieved from satellite measurements (Fisher et al. (2017)). However, almost all the schemes designed for this challenging task are diagnostic models relying more and more on the satellite measurements (Michel et al. (2016)). Major advances have been made in rainfall estimations from satellites (Zhou et al. (2014); Huffman et al. (2015)), but its use in continental and continuous monitoring in near-real time is still uncertain to this date for some applications (Anjum et al. (2016)). Therefore, evapotranspiration models may need empirical formula to diagnose the occurrence of interception, on the basis of already used input like air temperature and air humidity.

A few diagnostic models of interception exist in the literature, as it is needed as well in remote sensing evapotranspiration models as in epidemiology studies. In Fisher, Tu, and Baldocchi (2008) and Mu, Zhao, and Running (2011), the models make use of a fixed threshold on the air relative humidity (70%) to diagnose leaf wetness and triggers a specific module for calculation of evaporation from the interception reservoir. In plant disease science, a CART algorithm (Kim et al. (2002)) has been developed based on standard meteorological variables to derive leaf wetness duration, and consequently leaf wetness, identified to be an indicator for water interception on the vegetation canopy. This method, as well as threshold methods, have been further discussed by Bregaglio et al. (2011) in the view of plant disease.

In this study, we further investigated three empirical schemes validity by comparing them to canopy water interception forecasted by a global circulation model (GCM) that uses a Gash-based model, at 16 locations across Europe, Africa and South America, sampling representative climates and vegetation covers. The comparison revealed a good diagnostic efficiency of a simple threshold method on relative humidity, tuned differently for day and night, compared to the simulated presence of interception. Based on the GCM forecasted amount of interception, we present an optimized scheme to quantify the amount of water stored on canopies depending on relative air humidity levels.

As the presence of water stored on vegetation can have a significant impact on the total evapotranspiration given by the evapotranspiration models, the retrieved interception amount is implemented into a specific evapotranspiration model based on remote sensing derived data and ingested for the evapotranspiration calculation. In the following next two sections, we optimize and assess an empirical interception model, then evaluate the impact on evapotranspiration when plugged in an evapotranspiration satellite retrieval algorithm based on Meteosat satellite data.

## 2. Selecting a suitable empirical formulation for water interception on vegetation

### *2.1. Meteorological indicators & empirical models of detection of interception on canopies*

The meteorological variables that can be used by the methods are the air temperature at 2 m ($T$), the air humidity at 2 m, that can be given either by the dew point temperature ($T_d$), the specific humidity or the relative humidity ($H_r$), and at last the wind speed at 10 m above the surface ($W$). Those are standard measurements at meteorological stations and

are also input of the evapotranspiration model either retrieved from GCMs or from a network of ground meteorological stations or even from satellites.

Three models to detect presence of intercepted water have been considered. Method 1 is the simplest empirical model based on one single meteorological variable, the air relative humidity, $H_r$. Following Fisher, Tu, and Baldocchi (2008), a threshold of $H_r = 70\%$ can be considered as optimal to determine the presence of intercepted water on the vegetation, while no evidence of the success rate was previously reported in their study. Model 1 has been used in major evapotranspiration algorithms based on remote sensing data at continental scale (Fisher, Tu, and Baldocchi (2008); Mu, Zhao, and Running (2011)).

Model 2 is the CART model (Kim et al. (2002)), based on the evaluation of the dew point depression *DPD*, which is the difference between air temperature and air dewpoint temperature. Above a threshold of 3.7 K, the vegetation is considered dry. Under 3.7 K, it is either wet or dry depending on wind speed conditions (threshold of 2.5 $ms^{-1}$) and relative humidity (threshold of 87.8%). In cases of low wind/high relative humidity, inequality 1 and inequality 2 play a role in departing between wet and dry events. This method has been tested in plant disease studies and has shown a statistical superiority against other methods to predict leaf wetness for funghi spreading (Bregaglio et al. (2011)).

$$1.6000\sqrt{\mathrm{T}} + 0.0036T^2 + 0.1531H_r - 0.4599WDPD - 0.0030TH_r \geq 14.4674 \quad (1)$$

$$0.7921\sqrt{\mathrm{T}} + 0.0046H_r - 2.3889W - 0.039TW + 1.0613WDPD \geq 37.0 \quad (2)$$

Model 3 is a variant of model 1, where the threshold on relative humidity is tuned for night-time (including dew deposition on vegetation canopy) and daytime events separately, allowing the highest detection rate for both dry and wet vegetation in all considered locations. The optimization methodology is presented in the next subsections.

## 2.2. Assessment of the selected empirical formulations

### 2.2.1. Methodology

Meteorological forecasts from the European Centre for Medium-range Forecasts (ECMWF) ERA-Interim (Simmons et al. (2006)) at 16 locations over Europe, Africa and South America (listed in Table 1) are the input of the empirical models over the year 2007. The choice of meteorological forecasts from ECMWF GCM is fairly consistent with the typical settings of evapotranspiration models, as most of those models use GCM forecasts (Miralles et al. (2010); Ghilain, Arboleda, and Gellens-Meulenberghs (2011)) or analyses of standard

**Table 1.** List of stations used in this study.

| Dataset | Country | Dataset | Country |
|---|---|---|---|
| DE-Hai | Germany | FI-Hyy | Finland |
| BE-Lon | Belgium | ML-Ago | Mali |
| BE-Vie | Belgium | IL-Yat | Israel |
| IT-Col | Italy | SA-Sk1 | South Africa |
| IT-Roc | Italy | SA-Sk2 | South Africa |
| FR-Lam | France | BR-San | Brazil |
| ES-Lam | Spain | BR-Man | Brazil |
| IT-Lecc | Italy | SD-Dem | Demokeya |

meteorological variables as input. The output time series from the application of the empirical approaches described in the previous section is compared to the interception reservoir forecasted by ECMWF. The event is dry if the interception reservoir is empty or with a reservoir of less than a threshold (0.05 mm), it is considered wet otherwise. Note that the interception reservoir content is highly variable, as it can deplete very quickly, and fill up easily with rain events or dew depositions onto leaves.

For each scheme, contingency tables are created for each site with the true (success) and false (failure) rates in detecting interception and interception-free cases (Table 2). From contingency tables, it is possible to evaluate the success rates of the empirical models in detecting dry ($SR_D$) and/or wet ($SR_W$) periods, but also failures ($FR_D$ and $FR_W$). It is also informative to know how frequent dry and wet periods are comparatively. While dry periods are scarce in the Amazonian forest, it is quite the opposite for the semi-arid sites in Mali and Sudan, with very few wet events recorded during the simulation period. From the contingency tables, besides $SR_D$ and $SR_W$ that are normalized to the number of observed dry or wet period, an overall success rate is derived which combines both information and gives an overall performance of the considered models.

### 2.2.2. Tuning

Model 3 needs first to be tuned before being globally evaluated. For each threshold of relative humidity between 50% and 90%, $SR_D$, $SR_W$ and their mean value is computed for each dataset (Figure 1). The night dew deposition (Figure 2) and the day (Figure 1) events are separated for each dataset because different thresholds might appear. The mean value of both success rates is a good compromise to detect with a fair rate both situations. However, the threshold varies from one station to another. Those thresholds have been averaged, disregarding any differences in bioclimatic conditions: for day events ($H_r \geq 81\%$) and night events ($H_r \geq 88\%$).

### 2.2.3. Comparative evaluation

For each scheme (Model 1 to 3), the success rates for dry, wet and combined periods are represented in Figure 3. For model 1, there is a better performance to detect dry periods ($\geq$ 90%), probably with an overestimation of those cases. The agreement between 30% and 70% for wet cases, except for semi-arid regions (where there is small interception). If cases with only higher interception reservoir content are retained, the performances of detection are between 55% and 90%. Model 2 is generally outperformed by model 1 for dry cases, but not for wet cases. For model 3 (Figure 3), because of the tuning, results are better than for model 2 and 1. At most stations, there is an identification of 80% or more of dry events and wet events. The identification of dry events is a bit less efficient for brazilian sites (between 70% and 75%), and wet events for the semi-arid sites (Agoufou and Demokeya), for which very

**Table 2.** Example of table of contingency calculated for each model and each time series.

| | ERA-I Yes | ERA-I No |
|---|---|---|
| Model Yes | $SR_W$ | $FR_D$ |
| Model No | $FR_W$ | $SR_D$ |

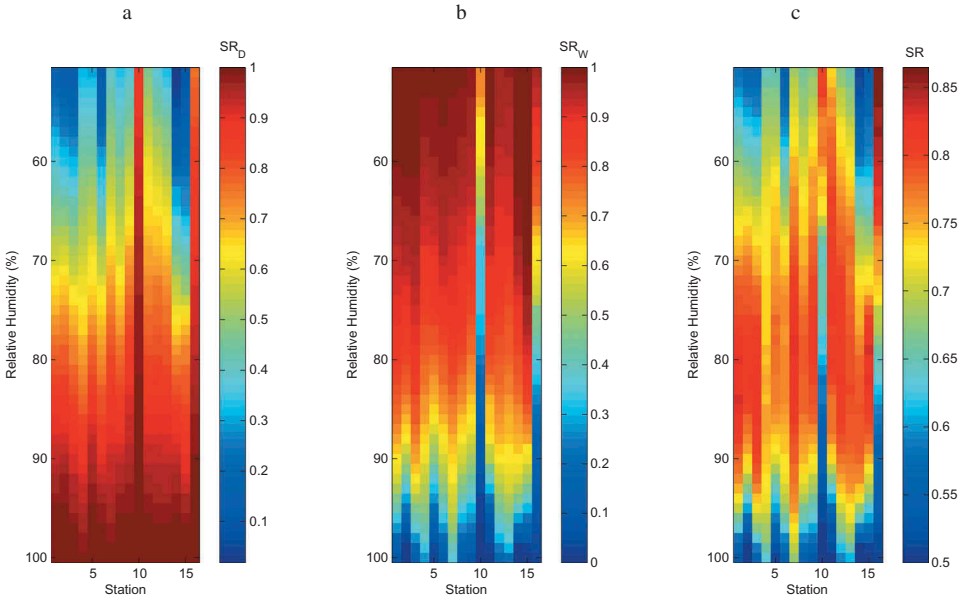


**Figure 1.** Performances of model 3 on diurnal events with thresholds on relative humidity ranging from 50% to 90% for dry (a), wet (b), and average of both cases (c).

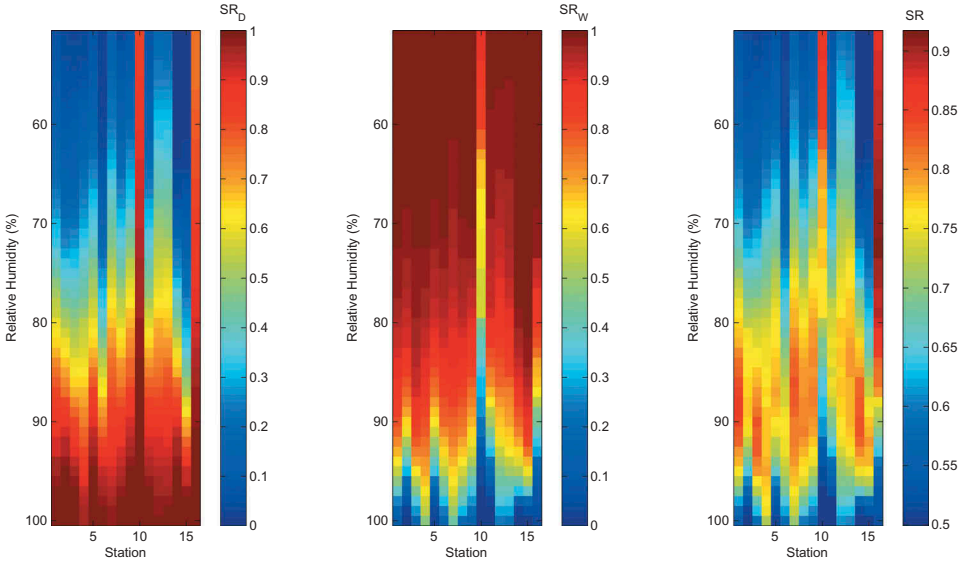


**Figure 2.** Same as in Figure 1, but for night events.

few wet events are detected. Model 3 achieves a diagnostic of interception presence with an acceptable success rate in most conditions superior to the two other models and can be easily used in evapotranspiration models.

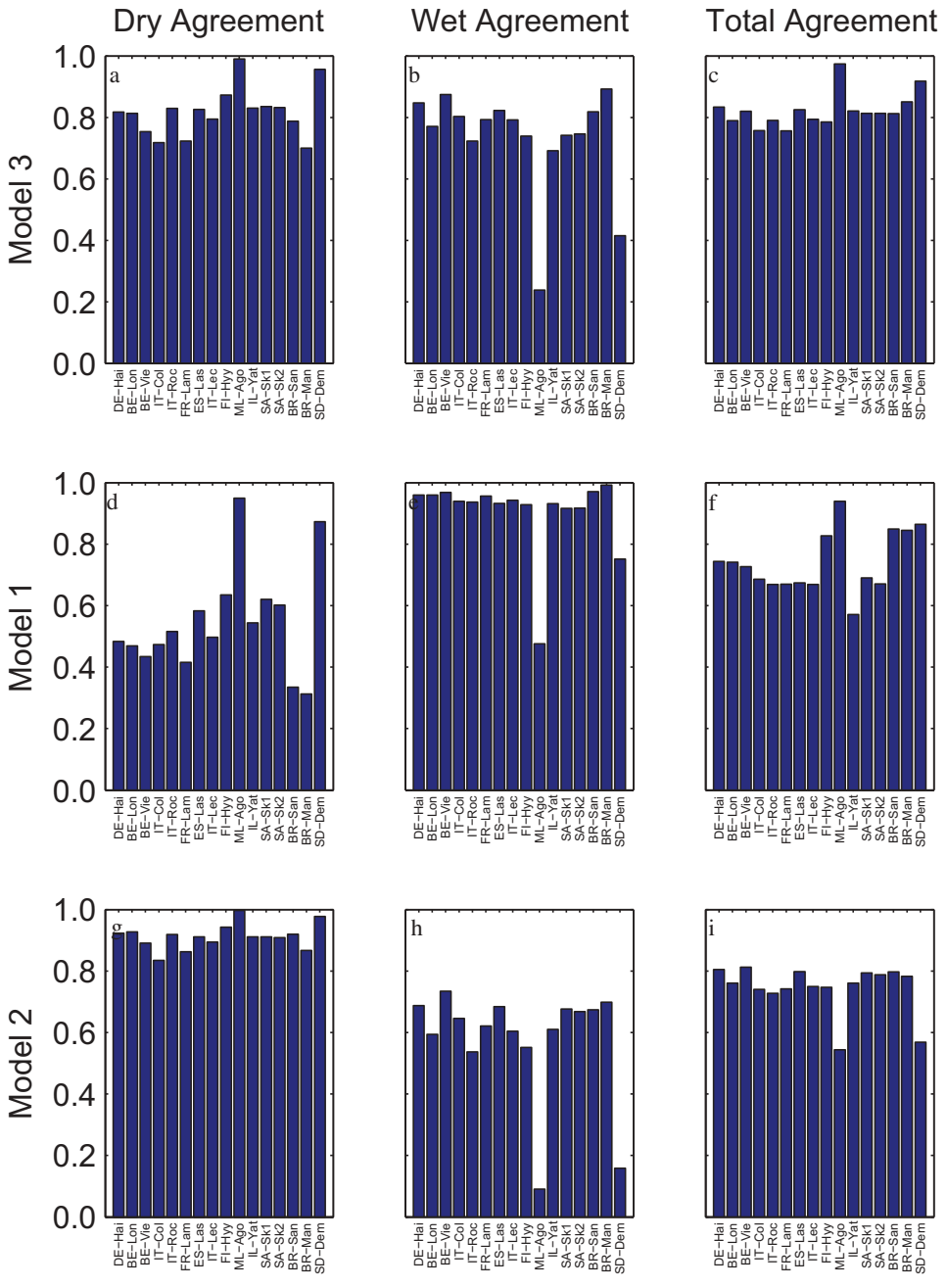


**Figure 3.** Percentage of agreement between ERA-interim and model 1, 2 and 3 results over the 16 stations, for dry, wet and both cases combined. Model 3 shows the best homogeneous scores regardless of the situation.

### *2.3. Linking the intercepted water volume to relative humidity of the air*

In the previous subsection, the results were limited to the detection of presence of interception triggered when a threshold on the intercepted water content of ECMWF

**Table 3.** Relative humidity thresholds for detecting interception (over the minimum water content, column 1), average success rates on 14 datasets, and success rate of the interception on the overall datasets using the same differentiated thresholds of column 2 and 3.

| | Minimum $H_r$ (%) | | Optimized SR | | |
|---|---|---|---|---|---|
| $W_{l,min}(mm)$ | Day | Night | Day | Night | SR (all, fixed threshold) |
| 0.05 | 80.86 | 88.43 | 80.68 | 81.22 | 80.52 |
| 0.10 | 84.28 | 89.64 | 81.17 | 79.13 | 80.37 |
| 0.20 | 87.93 | 91.64 | 82.38 | 80.03 | 80.62 |
| 0.30 | 90.46 | 92.62 | 83.00 | 80.73 | |
| 0.40 | 91.85 | 94.46 | 84.60 | 81.62 | |
| 0.50 | 93.25 | 95.50 | 85.69 | 81.65 | |

forecasts set to 0.05 mm is exceeded. Linking the amount of water intercepted to relative humidity would allow not only to detect presence of water but to quantify it. Thresholds of relative air humidity have therefore been calculated for different interception water storage amounts. The same contingency tables have been calculated for model 3 using a detection threshold on ECMWF interception of 0.1, 0.2, 0.3, 0.4 and 0.5 mm, respectively. For the diurnal events, it led to an optimal threshold on relative humidity of rising from 84.28% to 93.25% (Table 3), with success rates above 80% (having excluded the two Sahelian datasets for which statistics on wet events is not sufficient). For each minimum water amount stored on vegetation used for interception detection on ECMWF forecasts is associated two optimized relative humidity thresholds: one for night and the other for day. While rising the minimum of intercepted water for interception to be detected, the relative humidity threshold increases for both day and night events. The threshold for day events increases more drastically than for night events, increasing 7% of relative humidity during day events and 3% for night events. It must be noted here that the model 3 performs with a relatively constant success rate for all interception amounts.

Based on Table 3, the relative humidity of the air could be related to the amount of intercepted water $W_l$ (Figure 4). If air relative humidity was less than the first threshold, the interception amount was set to zero, while, when exceeding the last threshold, the content was set to 0.5 mm. Between the thresholds which represent the actual range of variation analysed, third-order and second-order polynomials have been fitted (Equations (3) and (4), for day and night, respectively).

$$W_l = 16.927.10^{-5}H_r^3 - 0.414.10^{-1}H_r^2 + 3.385H_r - 92.642 \quad (3)$$

$$W_l = 3.000.10^{-3}H_r^2 - 4.833.10^{-1}H_r + 19.536 \quad (4)$$

## 3. Impact on the evapotranspiration model estimates

### 3.1. The evapotranspiration model

The evapotranspiration model (Ghilain, Arboleda, and Gellens-Meulenberghs (2011)) of this study exploits the capabilities of the new imagery available from the SEVIRI instrument on-board the geostationary Meteosat Second Generation satellites every 15 min at a resolution between 3 and 5 km over Europe, Africa and South America to monitor this

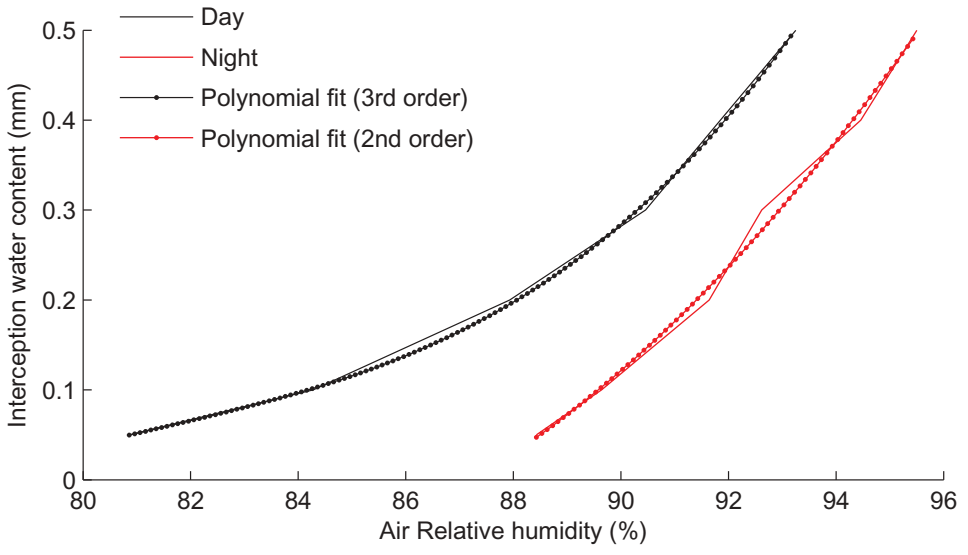


**Figure 4.** Relation between relative humidity thresholds and interception water amount, $W_I$ for day and night events can be approximated by polynomials. The threshold on relative humidity increases with the amount of water intercepted by vegetation, with lower thresholds required for day events.

crucial component of the water cycle over land. The model, called LSA-SAF ET in reference to its operational set-up (Trigo et al. (2011)), is a diagnostic model, based on the formulation of a land surface model, driven by radiation components and biophysical variables derived from the satellite data, and short-term forecasts of atmospheric surface variables provided by ECMWF, more specifically the air temperature, air humidity, wind speed at screen-level. A resistance approach has been adopted in the model to compute the evapotranspiration for every spatial unit and sub-elements grouped by vegetation types every 30 min. Interception of water by the canopy was not accounted for in the first operational set-up.

### 3.2. Implementation into LSA-SAF ET model

The baseline implementation follows the approach of assigning an interception *tile* for the entire grid cell, when the first relative humidity threshold is exceeded. Similarly as in Fisher, Tu, and Baldocchi (2008) and Mu, Zhao, and Running (2011), a switch is inserted in the LSA-SAF ET algorithm: before the energy balance evaluation, relative humidity is compared to the threshold; if it exceeds, the vegetation tiles are set to wet by changing the stomatal resistance to zero allowing the computation of a potential water evaporation. This approach differs from using an open water tile, as vegetation parameters like roughness lengths are conserved, which accounts for a proper attenuation of wind speed by vegetation canopy.

An alternative implementation, consistent with land surface models, is to assign a fraction of the grid cell to the interception depending on the amount stored on the canopy calculated by the polynomial relations derived above. The use of a fraction of the grid cell occupied by interception is corresponding to realistic situations, as we expect for

small amount of intercepted water that mostly the upper layer of the canopy will be wet. This is supported by Czikowsky and Fitzjarrald (2009), who have found that during and after rain events in the Amazonian forests, interception involves approximately 40% of the canopy, leaving more than a half dry. In TESSEL land surface model used at ECMWF, this interception water content is compared to a maximum reservoir content for the determination of the grid cell fraction covered by interception. The maximum storage of water in a grid cell (m) is function of leaf area index (LAI) (Eq 5), where PCBS, PCHV and PCLV represent the fraction covered by bare soil, high vegetation and low vegetation.

$$W_{\mathrm{i,max}} = 0.0002[\mathrm{PC_{BS}} + \mathrm{PC_{HV}}.\mathrm{LAI}(\mathrm{PC_{HV}}) + \mathrm{PC_{LV}}.\mathrm{LAI}(\mathrm{PC_{LV}})] \quad (5)$$

The fraction occupied by wet leaves is computed as the ratio of $W_I$ with $W_{I,max}$, cut high at 1. Therefore, using the threshold of 0.05 mm, the fraction of interception computed with such model is minimum 25%, 10% and 1% for LAI of 1, 3 and 5 $m^2$ $m^{-2}$ respectively. Comparatively to the baseline implementation, the switch cannot be complete, as only a fraction of the canopy is considered to be wet. First, the fraction occupied by the interception must be computed from the relative humidity and the LAI. Then, in order to alter as less as possible the algorithm, a weighted average of the vegetation type resistance and null resistance for the fraction of interception is taken for the computation of evapotranspiration.

### 3.3. Impact on the evapotranspiration model results

A test case for each sub-window has been chosen to assess quantitatively the change on LSA-SAF ET results. For Europe, Southern Africa and South America, time slot at 12:00 UT in August 2011, the 17 August for South America and South Africa and the 19 August for Europe were chosen. For Northern Africa, the 27 May 2007 was chosen. August corresponds to a period of the year with possible large convective rainfall rates all across Europe, while the evaporative demand is very high due to solar radiation. In Southern Africa, it is approximately the dry season, with very few rainfalls observed. The month of May in Northern Africa is set during the wet season across sub-sahelian Africa, while still at the end of the dry season in Sahel (the rainy season tends to fall a bit later, around July).

With the first implementation scheme, a clear impact is seen over Northern Europe, at places where clouds impact the solar radiation, with an evapotranspiration rate almost twice the result without interception. Points with very high differences are also found in coastal pixels, possibly due to the inclusion of some higher humidity ocean values in the grid cells retained for spatial interpolation of ECMWF forecasts of air temperature and dew point temperature onto the satellite grid. Over northern Africa, differences are noticeable near the equator (a 40% change), as well as in the coastal areas of west Africa. Also, the evapotranspiration is 30% to 40% larger over some regions of eastern equatorial Africa, where dense forests are (eg. Kenyan coast). A few changes are observed for Southern Africa, especially near the equator (changes around 30% and 60%) and over Madagascar wind forest (up to 100% change). Because August is mostly the dry season across Southern Africa, and that particular date is very dry, only a few cases are observed. The largest changes are found for South America, mostly around the equator and the Amazonian river basin, where changes between 50% and 60% are observed. In absolute

value, those changes account for approximately 0.2 mm $hr^{-1}$. This large absolute value corresponds to morning value, and is expected to be higher at noon, at the maximum of solar radiation.

The same slots have been reprocessed using the alternative implementation scheme, which consists in relating relative humidity and LAI to a fraction occupied by interception on the vegetation. The results (Figure 5(c)) show a reduced difference (about 50%) compared to the effect of the first scheme.

Evapotranspiration data are very scarce to support the observed changes, as it remains difficult to measure accurately energy fluxes during rain events. However, new techniques have been developed to analyse eddy flux data in view to detect rainfall interception (Czikowsky and Fitzjarrald (2009)). The authors found over the amazonian forest an evaporative fraction approximately 15% higher during rainy days than dry days and revealed that interception detection does not necessarily imply that the total canopy is

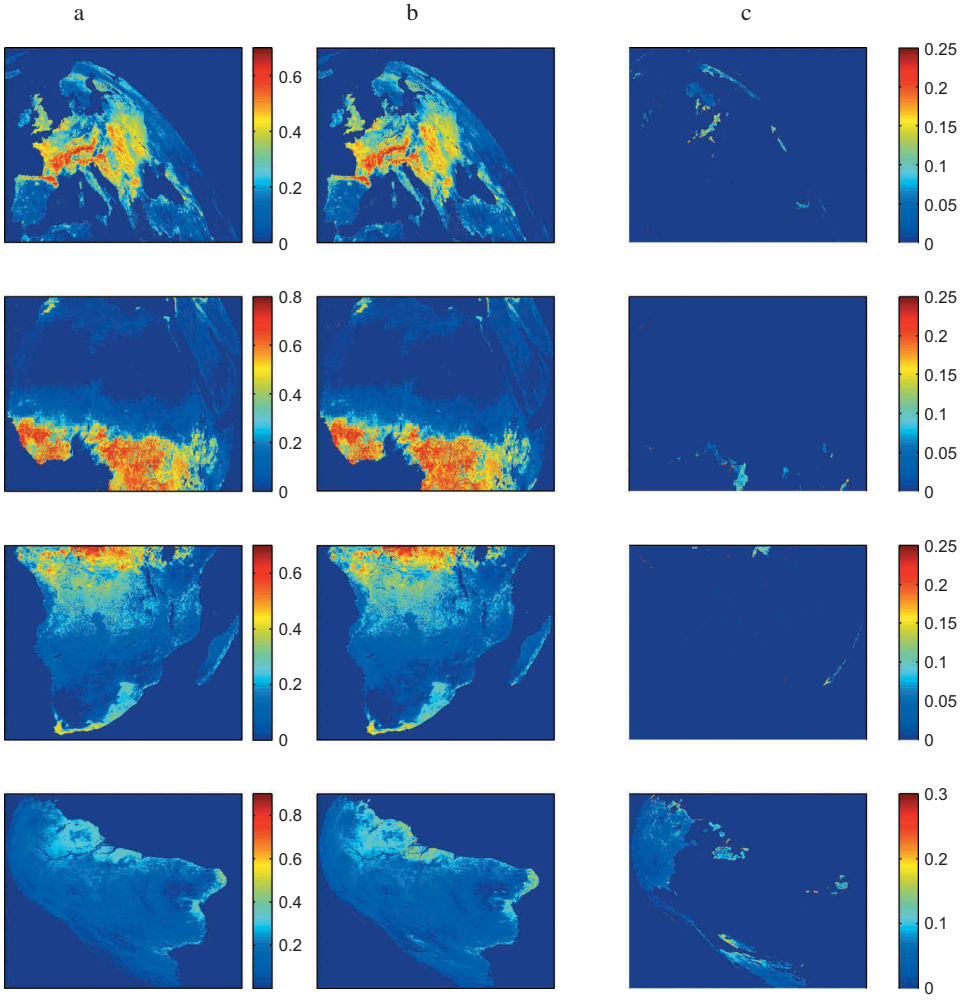


**Figure 5.** Result of LSA-SAF ET v4.1.0 for Europe on 2011-08-19 at 12:00 UT (a), with the inclusion of the % of interception (b), and the difference between both results (c), in mm $hr^{-1}$ (option 2).

wet. Analysing the excess of evapotranspiration measured by eddy covariance, they found that the application of the Penman–Monteith formula commonly used in evapotranspiration models with a zero resistance of the plant to release of water vapour was far from being realistic. By inverting the flux measured, a resistance of 40 s $m^{-1}$ is found. However, as an approximation, the zero resistance approach could be used if the fraction of wet canopy is adapted: they found that in average 40% of the canopy is wet during and after rain events. This latter observation suggests that considering a full pixel unit evaporating at the potential rate may be exaggerated compared to what is actually measured in such forests, which should correspond to only 40% of wet canopy and an excess of 15% to what is currently observed in dry periods. These latter observations are in closer agreement with the proposed alternative implementation to compute evapotranspiration over wet canopies, as only a fraction of the canopy contributes to the potential evaporation rate and the excess is about 25–30%.

## 4. Conclusion

We evaluated how efficiently water interception by vegetation could be diagnosed from standard meteorological variables used by most remote sensing based evapotranspiration models applied at continental scale. A threshold on the relative humidity of the air, differentiated between day ($H_r \geq 81\%$) and night ($H_r \geq 88\%$), allows a simple and efficient detection of the water interception with a success rate compared to a numerical Gash-based model of more than 80% in almost every situation. Considering increasing thresholds, we established polynomial relations between the relative humidity and the amount of water intercepted by the vegetation, and therefore the fractional coverage of interception compared to dry vegetation. The scheme was easily implemented into an evapotranspiration model based on remote sensing data without the explicit use of any additional input variable. This is of considerable interest for the time being as most models do not involve time-evolving equations.

The scheme is implemented in the evapotranspiration model based on Meteosat data as a simple switch for the calculation of the energy balance at the tile level, which is activated when the relative humidity exceeds a given threshold and substitute the vegetation stomatal resistance by zero (unconstrained). The impact has been evaluated on test cases, showing little to moderate changes over areas in Europe and Africa, but large changes over South America and especially over the Amazon river basin.

The scheme selected here is a good candidate for estimating the portion of grid cells where evaporation from water intercepted by canopies occurs. It is therefore recommended for diagnostic evapotranspiration models based on remote sensing data.

## Disclosure statement

No potential conflict of interest was reported by the authors.

## Funding

This work was supported by the Belgian Federal Science Policy Office [ESA/PRODEX C4000110695]; EUMETSAT [LSASAF project].

## References

Anjum, M. N., Y. Ding, D. Shangguan, M. W. Ijaz, and S. Zhang. 2016. "Evaluation of High-Resolution Satellite-Based Real-Time and Post-Real-Time Precipitation Estimates during 2010 Extreme Flood Event in Swat River Basin, Hindukush Region." *Advances in Meteorology* 2016 (Article ID 2604980): 8. doi:10.1155/2016/2604980.

Bregaglio, S., M. Donatelli, R. Confalonieri, M. Acutis, and O. Orlandini. 2011. "Multi Metric Evaluation of Leaf Wetness Models for Large Area Application of Plant Disease models." *Agricultural and Forest Meteorology* 151: 1163–1172. doi:10.1016/j.agrformet.2011.04.003.

Czikowsky, M. J., and D. R. Fitzjarrald. 2009. "Detecting Rainfall Interception in an Amazonian Rain Forest with Eddy Flux Measurements." *Journal of Hydrology* 377: 92–105. doi:10.1016/j.jhydrol.2009.08.002.

Fisher, J. B., F. Melton, E. Middleton, C. Hain, M. Anderson, R. Allen, M. F. McCabe, et al. 2017. "The Future of Evapotranspiration: Global Requirements for Ecosystem Functioning, Carbon and Climate Feedbacks, Agricultural Management, and Water Resources." *Water Resources Research* 53: 2618–2626. doi:10.1002/2016WR020175.

Fisher, J. B., K. P. Tu, and D. D. Baldocchi. 2008. "Global Estimates of the Land-atmosphere Water Flux Based on Monthly AVHRR and ISLSCP-II Data, Validated at 16 FLUXNET Sites." *Remote Sensing of Environment* 112 (3): 901–919. doi:10.1016/j.rse.2007.06.025.

Gash, J. H. C. 1979. "An Analytical Model of Rainfall Interception in Forests." *Quarterly Journal of the Royal Meteorological Society* 105: 43–55. doi:10.1002/qj.49710544304.

Ghilain, N., A. Arboleda, and F. Gellens-Meulenberghs. 2011. "Evapotranspiration Modelling at Large Scale Using Near-real Time MSG SEVIRI Derived Data." *Hydrology and Earth System Sciences* 15: 771–786. doi:10.5194/hess-15-771-2011.

Huffman, G. J., D. T. Bolvin, D. Braithwaite, K. Hsu, R. Joyce, C. Kidd, E. J. Nelkin, and P. Xie. 2015. "Algorithm Theoretical Basis Document (ATBD) Version 4.5. NASA Global Precipitation Measurement (GPM) Integrated Multi-satellitE Retrievals for GPM (IMERG) NASA."

Kim, K. S., S. E. Taylor, M. L. Gleason, and K. J. Koehler. 2002. "Model to Enhance Site-specific Estimation of Leaf Wetness Duration." *Plant Disease* 86: 179–185. doi:10.1094/PDIS.2002.86.2.179.

Michel, D., C. Jimenez, D. G. Miralles, M. Jung, M. Hirschi, A. Ershadi, B. Martens, et al. 2016. "The WACMOS-ET Project Part 1: Tower-scale Evaluation of Four Remote-sensing-based Evapotranspiration Algorithms." *Hydrology and Earth System Sciences* 20: 803–822. doi:10.5194/hess-20-803-2016.

Miralles, D. G., J. H. Gash, T. R. H. Holmes, R. A. M. de Jeu, and A. J. Dolman. 2010. "Global Canopy Interception from Satellite Observations." *Journal of Geophysical Research* 115: D16122. doi:10.1029/2009JD013530.

Mu, Q., M. Zhao, and S. W. Running. 2011. "Improvements to a MODIS Global Terrestrial Evapotranspiration Algorithm." *Remote Sensing of Environment* 115: 1781–1800. doi:10.1016/j.rse.2011.02.019.

Simmons, A., S. Uppala, D. Dee, and S. Kobayashi. 2006. "ERA-Interim: New ECMWF Reanalysis Products from 1989 Onwards." *ECMWF Newsletter* 10: 26–35.

Trigo, I. F., C. C. DaCamara, P. Viterbo, J.-L. Roujean, F. Olesen, C. Barroso, F. Camacho-de Coca, et al. 2011. "The Satellite Application Facility on Land Surface Analysis." *International Journal of Remote Sensing* 32 (10): 2725–2744. doi:10.1080/01431161003743199.

Zhou, T., B. Nijssen, G. J. Huffman, and D. P. Lettenmaier. 2014. "Evaluation of Real-time Satellite Precipitation Data for Global Drought Monitoring." *Journal of Hydrometeorology* 15: 1651–1660. doi:10.1175/JHM-D-13-0128.1.